

# Theory of Electromotive Force Induced by Domain Wall Motion

Shengyuan A. Yang, Di Xiao, and Qian Niu

*Department of Physics, The University of Texas, Austin, Texas, 78712-0264, USA*

(Dated: February 28, 2019)

We formulate a theory on the dynamics of conduction electrons in the presence of moving magnetic textures in ferromagnetic materials. We show that the variation of local magnetization in both space and time give rise to topological fields, which induce electromotive forces on the electrons. Universal results are obtained for the voltage drops induced by both transverse and vortex domain walls traveling in a magnetic film strip, and their measurement may provide clear characterization on the motion of such walls.

PACS numbers: 75.75.+a 72.25.Ba 75.47.-m 75.60.Ch

The interplay between electron transport and magnetic dynamics is a central problem of spintronics research. It has been known that the presence of a domain wall can change the electrical resistance of a ferromagnetic conductor [1, 2, 3, 4]. It has also been demonstrated that an electric current can drive a domain wall motion through coupling between the conduction electrons and the local magnetic moments [5, 6, 7, 8, 9, 10, 11, 12, 13, 14, 15]. The reverse of this effect, i.e., electron transport induced by a moving domain wall, has been proposed by Berger [16] based on phenomenological arguments. Anticipating experimental studies of this important phenomenon, a general microscopic theory is highly desirable to underpin these predictions and to provide precise guidance to the experiments.

In this Letter, we provide such a theory within the framework of semiclassical dynamics of electrons in a magnetic background which varies slowly both in space and time. Indeed, the width of a typical domain wall in a ferromagnetic nanowire is about a few hundred nanometers, which is much larger than the electron Fermi wavelength, and the domain wall speed is much smaller than the electron speed. One can therefore consider the adiabatic limit where the spin of the conduction electrons follow the direction of local magnetization vector. We find that Berry phase terms [17] enter into the equation of motion as a pair of topological fields, acting like electric and magnetic fields on the electrons.

Our theory is applied to two domain wall configurations. For the transverse wall, we reproduce the result of the AC ferro-Josephson effect proposed by Berger [16]. For the vortex wall, depending on the applied magnetic field, the vortex core takes a linear (small field) or a zigzag (high field) motion. We predict both a longitudinal and transverse voltage for the zig-zag motion, with universal results which may be used to provide clear characterization of the vortex motion. Extra voltage due to nonadiabatic effects is also estimated at the end of the paper, and is found to be subdominant.

To construct our theory, we consider a ferromagnetic thin film, which is taken to be the x-y plane. The time evolution of local magnetization can be driven by a uni-

form external magnetic field (x-direction). Our model Hamiltonian then takes the following form,

$$\hat{H} = \hat{H}_0[\mathbf{q} + (e/\hbar)\mathbf{A}(\hat{\mathbf{r}})] - J\mathbf{M}(\hat{\mathbf{r}}, t) \cdot \hat{\boldsymbol{\sigma}} - \hbar\hat{\sigma}_x. \quad (1)$$

The first term is the bare Hamiltonian for the conduction electrons,  $\mathbf{q}$  is the Bloch wave-vector, and  $\mathbf{A}(\mathbf{r})$  is the vector potential of the external magnetic field. The second term is the *s-d* coupling between a conduction electron and the local d-electron magnetization  $\mathbf{M}(\mathbf{r}, t)$ , and  $J$  is the s-d coupling strength. The last term represents the Zeeman coupling between electron and the external magnetic field, with  $\hbar = \frac{1}{2}g_s\mu_B B$ .

To apply the semiclassical wave-packet formalism for the conduction electrons [18], we first write down the local Hamiltonian at the center position of the electron wave-packet  $\mathbf{r}_c$ ,

$$\hat{H}_c = \hat{H}_0[\mathbf{q} + (e/\hbar)\mathbf{A}(\mathbf{r}_c)] - K(\mathbf{r}_c, t)\mathbf{n}(\mathbf{r}_c, t) \cdot \hat{\boldsymbol{\sigma}}, \quad (2)$$

where  $\mathbf{n}(\mathbf{r}_c, t)$  is the unit vector of the exchange plus Zeeman field, while  $K(\mathbf{r}_c, t)$  is its strength. To deal with the vector potential, as discussed by Sundaram and Niu, we introduce the gauge invariant crystal momentum  $\mathbf{k} = \mathbf{q} + (e/\hbar)\mathbf{A}(\mathbf{r})$ . For ferromagnetic materials with  $J \sim 1\text{eV}$ , we may only consider the majority carriers whose spins are polarized along  $\mathbf{n}(\mathbf{r}_c, t)$ . This position and time dependence of the spin wave function gives rise to Berry curvatures in space and time, which can affect the dynamics of an electron wavepacket. More specifically, we find that the equations of motion for the wavepacket center as (subscript *c* is dropped here)

$$\dot{\mathbf{r}} = \frac{\partial \mathcal{E}_0}{\hbar \partial \mathbf{k}}, \quad (3)$$

$$\dot{\mathbf{k}} = \frac{\partial K}{\hbar \partial \mathbf{r}} - \frac{e}{\hbar} \dot{\mathbf{r}} \times \mathbf{B} - \dot{\mathbf{r}} \times \mathbf{C} - \mathbf{D}, \quad (4)$$

where  $\mathcal{E}_0$  is the Bloch band energy for  $\hat{H}_0$ . Originated from Berry curvatures in real space, two new fields  $\mathbf{C}$  and  $\mathbf{D}$  appear in the equations of motion. They are entirely due to the spatial and temporal variation of local spin

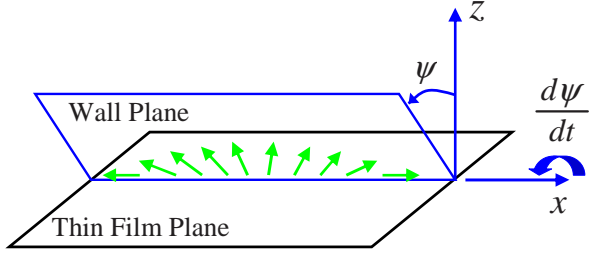


FIG. 1: (color online). Schematic picture of a tail-to-tail transverse domain wall. The magnetization direction changes within a wall plane which makes an angle  $\psi$  with vertical direction.

textures. In terms of the spherical angles  $(\theta, \phi)$  specifying the direction of  $\mathbf{n}$ , the fields  $\mathbf{C}$  and  $\mathbf{D}$  are given by

$$\mathbf{C}(\mathbf{r}, t) \equiv \frac{1}{2} \sin \theta (\nabla \theta \times \nabla \phi), \quad (5)$$

$$\mathbf{D}(\mathbf{r}, t) \equiv \frac{1}{2} \sin \theta \left( \frac{\partial \phi}{\partial t} \nabla \theta - \frac{\partial \theta}{\partial t} \nabla \phi \right). \quad (6)$$

Field  $\mathbf{C}$  is similar to the gyrovector used in the discussion of Bloch line dynamics [19]. From their appearance in equation (4), we observe that  $\mathbf{C}$  acts like a magnetic field while  $\mathbf{D}$  behaves like an electric field. This point will be further explored below.

Apply these formulas to the one-dimensional domain wall case where  $\theta$  and  $\phi$  only depend on coordinate  $x$  of the 2D plane. Then  $\mathbf{C} = 0$  and  $\mathbf{D} = D\mathbf{e}_x$ . For a transverse domain wall in the absence of external magnetic field, the local spins rotate within the 2D plane with the profile  $\theta = \pi/2$  and  $\phi(x) = \cos^{-1} \tanh[(x - X)/\lambda]$ , where  $X$  denotes the center of the domain wall and  $\lambda$  is the domain wall width [19]. When an external  $\mathbf{B}$  field is applied, not only will the domain wall propagate, but the local spins will also get tilted out of the x-y plane. As shown in Fig.1, these spins still lie within a "wall plane" which makes an angle  $\psi$  with the vertical direction. Below Walker's breakdown field, this plane is fixed, and the angles  $\theta$  and  $\phi$  are functions of  $(x - vt)$ , which makes  $\mathbf{D} = 0$ . Above Walker's breakdown field, this plane changes with time (with rate denoted by  $d\psi/dt$ ) [19], which leads to a non-zero  $\mathbf{D}$  field.

If the system is bounded electrically, in steady state, the domain-wall induced adiabatic force  $\hbar(\partial K/\hbar \partial x - D)$  must be balanced by the gradient of electrochemical potential. The voltage drop along the direction of domain wall motion is then

$$V_x = \frac{\hbar}{e} \int \left( D - \frac{\partial K}{\hbar \partial x} \right) dx = -\frac{\hbar}{e} \left( \frac{d\psi}{dt} + \frac{2\hbar}{e} \right). \quad (7)$$

In the calculation, we use the condition  $|h| \ll |J|$ , which is usually the case in experiments on ferromagnetic materials. The first term on the right hand side above represents the so-called *AC ferro-Josephson effect* proposed

by Berger in 1986 based on phenomenological considerations [16]. The additional term proportional to the field is due to the difference in Zeeman energy on the two sides of the domain wall, which should appear when we suddenly turn on the external field. However, since the spin relaxation time  $\tau_s \sim 10^{-12}$ s is much shorter than the characteristic time for domain wall motion, the voltage associated with this term cannot be measured in experiment [20].

Depending on the thickness and the width of the system, a magnetic domain wall in a thin film can also take a vortex structure [21]. In fact, most of the experiments done so far involve vortex walls rather than transverse walls. In the following, we apply the formula developed above to study the case of a single vortex in a nanowire. Assume that the vortex profile is characterized by a core radius  $a$ , which is about a few nanometers, and an outer radius  $R$ , which is comparable to the wire width  $w$ . For a positively polarized vortex centered at  $\mathbf{X}(t)$ , we may approximately write  $\theta = \frac{\pi}{2} [1 - \exp(-|\mathbf{r} - \mathbf{X}(t)|/a)]$  for  $|\mathbf{r} - \mathbf{X}| < R$  and  $\theta = \frac{\pi}{2}$  beyond the large radius, while for a negatively polarized vortex,  $\theta = \frac{\pi}{2} [1 + \exp(-|\mathbf{r} - \mathbf{X}(t)|/a)]$ . In both cases, we have  $\phi = \text{Arg}(\mathbf{r} - \mathbf{X}(t)) + \zeta \frac{\pi}{2}$  for  $|\mathbf{r} - \mathbf{X}| < R$ .  $\zeta = \pm 1$  indicates the chirality of the vortex. For a steady state motion of the vortex,  $\theta$  and  $\phi$  are functions of  $(\mathbf{r} - \mathbf{v}t)$ , where  $\mathbf{v} = \dot{\mathbf{X}}$ . Then

$$\mathbf{D} = -\frac{1}{2} \sin \theta [(\mathbf{v} \cdot \nabla \phi) \nabla \theta - (\mathbf{v} \cdot \nabla \theta) \nabla \phi] = \mathbf{C} \times \mathbf{v}, \quad (8)$$

Where the last equality resembles the relation between  $\mathbf{E}$  and  $\mathbf{B}$  fields. Because  $a \ll R \sim w$ , these fields are concentrated within the core region, where

$$\mathbf{C} = \frac{\pi}{4ar} e^{-r/a} \cos\left(\frac{\pi}{2} e^{-r/a}\right) \hat{\mathbf{e}}_z, \quad (9)$$

and  $\mathbf{D}$  is obtained by Eqn.(8). An important property of the  $\mathbf{C}$  field is that its total flux is a constant, i.e.,

$$\int \mathbf{C} d^2r = \frac{1}{2} \int \sin \theta d\theta d\phi \hat{\mathbf{e}}_z = \pi \hat{\mathbf{e}}_z. \quad (10)$$

which is topological—independent of the detailed profile of the vortex.

The two-dimensional character of the vortex domain wall makes the calculation of the induced voltage drop a bit complicated. Unlike the one-dimensional transverse wall case, the force field  $\mathbf{D}$  now has a curl. The gradient of the electrochemical potential can only cancel the curl-less part of this force field. Therefore, we need to solve the Poisson equation  $\nabla^2 V = (\hbar/e) \nabla \cdot \mathbf{D}$  with Neumann boundary condition (no current leaving the sample). It is seen that the effect of the  $\mathbf{D}$  field may be regarded as that of an electric dipole, whose spatial extension is of the size of the vortex core. The net dipole moment is equivalently given by the integral of the  $\mathbf{D}$  field times  $\hbar \epsilon_0/e$ . With

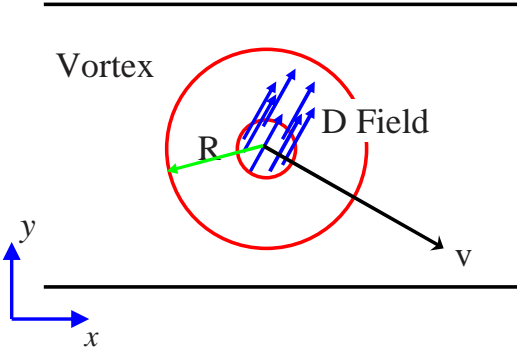


FIG. 2: (color online). Schematic picture of the  $\mathbf{D}$  field for a moving vortex.  $\mathbf{D}$  field is perpendicular to the vortex velocity and vanishes outside the core.

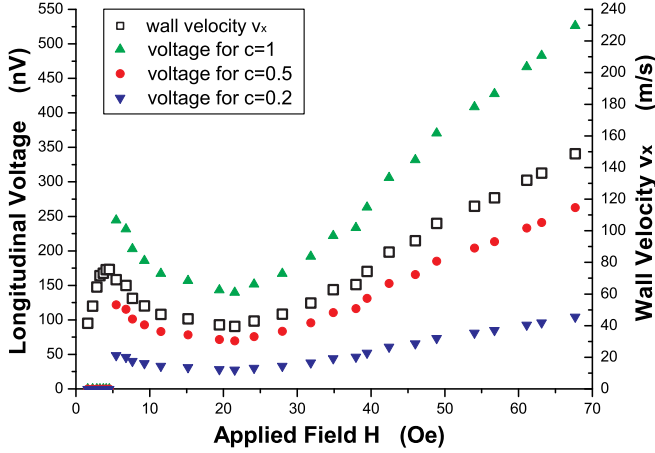


FIG. 3: (color online). Numerical results for longitudinal voltage associated with the vortex motion. The mobility curve is experimentally measured in [26]. It is assumed that  $v_y = cv_x$  here.

the help of Eqn.(8) and (10),  $\mathbf{p} = \varepsilon_0 \pi (\hbar/e) \hat{\mathbf{e}}_z \times \mathbf{v}$ , which is also a topological property of the vortex.

Another complication arises from the Magnus force on a moving vortex which pushes it in the transverse direction [22, 23]. At low fields, this Magnus force is balanced by the confining potential of the nanowire such that steady motion is still along x-direction. In this case, the source term of the Poisson equation resembles an electric dipole pointing along the y-direction, so the longitudinal voltage drop is expected to vanish in this case (barring nonadiabatic effects). At high fields, the confining potential can no longer balance the Magnus force and the vortex will begin a transverse motion. From the relation  $\mathbf{D} = \mathbf{C} \times \mathbf{v}$ , we observe that the dipole source within the vortex core gets rotated to acquire a finite x component. This makes the longitudinal voltage drop nonzero [Fig.2].

Analytical expression for the voltage drop can be obtained within a point-dipole approximation and using the image charge method. The longitudinal voltage drop is

obtained as,

$$V_x = -\pi \frac{\hbar}{e} \frac{v_y}{w}. \quad (11)$$

It is proportional to the transverse velocity, and inversely proportional to the wire width. In fact, this result is exact beyond the point-dipole approximation so long as the core is contained within the width and is far from the two ends of the sample as confirmed by numerical calculations. Measurement of this universal result may provide clear characterization of the vortex motion.

When the vortex hits one edge, the vortex domain wall transforms into a transverse domain wall [13, 24]. There is a range of external field under which this transverse wall propagates and generates a voltage according to Eqn.(7). But more probably, another vortex with a negative polarization will be emitted from this edge, travel across the wire and hit the other edge [24]. Hence the trajectory of the vortex assumes a zigzag type. During this process, chirality of the vortex is conserved [25], while both  $\mathbf{C}$  field and  $v_y$  change sign, so  $V_x$  remains unchanged during the vortex motion.

The sample used in the experiment of [26] has a width  $w = 600\text{nm}$  and a length of  $20\mu\text{m}$ . We assume the vortex has a core radius  $a = 10\text{nm}$ , an outer radius  $R = 200\text{nm}$ , and the average speed  $v_y$  is proportional to  $v_x$  for  $H > H_W$ , i.e.  $v_y = cv_x$  for some constant  $c$ . Then we calculate  $V_x$  as a function of  $H$  for  $c = 1, 0.5$  and  $0.2$  respectively. The results are plotted in Fig.3 together with the measured mobility curve from [26]. We observe the longitudinal voltage is vanishingly small below Walker breakdown ( $H_W \sim 40\text{Oe}$ ) and is proportional to  $v_x$  above Walker breakdown.

The motion of the vortex also induces a transverse voltage, which can also be calculated from the Poisson equation. Again using the method of image charge, for a vortex at the center of the wire, the transverse voltage at the longitudinal position of the vortex is found to be

$$V_y = \pi \frac{\hbar}{e} \frac{v_x}{w}. \quad (12)$$

When measured through a pair of lateral leads, one should observe a pulse of transverse voltage with the above peak value and with a time width determined by the wall speed and lead width. Oscillations can occur within this pulse above the breakdown field when the vortex executes zigzag motion. Each time the vortex collides with a sample edge and gets reflected with a change of polarization,  $V_y$  will change sign. Numerical calculations also confirm these findings. Therefore, by timing the transverse voltage pulse, one can determine the position and speed of the domain wall. And by measuring the frequency of the oscillations, one can detect the zigzag motion of the vortex.

Finally, we give an estimation of the extra voltage due to nonadiabatic effects. Although its microscopic origin is not clear at present, estimation can be done from

force balance considerations [5]. This voltage drop can be written as  $V_x^{na} = 2M_s R_0 \mu_i^{-1} v_x$ , where  $R_0$  is the ordinary Hall coefficient and  $\mu_i$ , called the intrinsic wall mobility, is a measure of the electrons' contribution to the viscous damping force on the domain wall. For permalloy thin films,  $M_s = 8 \times 10^5 \text{ A/m}$ ,  $R_0 = -1.4 \times 10^{-10} \text{ m}^3/\text{C}$  and  $\mu_i \simeq 2 \text{ m}^2/\text{C}$ . Assuming  $v_y \simeq v_x$ , then  $V_x^{na}$  is about 20 times smaller than the adiabatic voltage drop above breakdown. However, it is the dominant contribution to longitudinal voltage below breakdown.

The authors would like to thank Changhai Xu, Weidong Li, Chih-Piao Chuu, Wang Yao, Dennis P. Clougherty, Shufeng Zhang, Geoffrey S. D. Beach, Maxim Tsoi and James L. Erskine for valuable discussions. This work is supported by the NSF Grant No. DMR-0404252.

- 
- [1] J. F. Gregg, W. Allen, K. Ounadjela, M. Viret, M. Hehn, S. M. Thompson, and J. M. D. Coey, Phys. Rev. Lett. **77**, 1580 (1996).
  - [2] G. Tatara and H. Fukuyama, Phys. Rev. Lett. **78**, 3773 (1997).
  - [3] R. P. van Gorkom, A. Brataas, and G. E. W. Bauer, Phys. Rev. Lett. **83**, 4401 (1999).
  - [4] V. K. Dugaev, J. Barnas, A. Łusakowski, and L. A. Turski, Phys. Rev. B **65**, 224419 (2002).
  - [5] L. Berger, J. Appl. Phys. **55**, 1954 (1984).
  - [6] G. Tatara and H. Kohno, Phys. Rev. Lett. **92**, 086601 (2004).
  - [7] Z. Li and S. Zhang, Phys. Rev. B **70**, 024417 (2004); Phys. Rev. Lett. **92**, 207203 (2004).
  - [8] S. Zhang and Z. Li, Phys. Rev. Lett. **93**, 127204 (2004).
  - [9] A. Thiaville, J. Miltat and J. Vernier, J. Appl. Phys. **95** 7049 (2004).
  - [10] A. Thiaville, Y. Nakatani, J. Miltat, and Y. Suzuki, Europhys. Lett. **69**, 990 (2005).
  - [11] Z. Li, J. He, and S. Zhang, J. Appl. Phys. **99**, 08Q702 (2006).
  - [12] A. Yamaguchi, T. Ono, S. Nasu, K. Miyake, K. Mibu, and T. Shinjo, Phys. Rev. Lett. **92**, 077205 (2004).
  - [13] M. Kläui, P.-O. Jubert, R. Allenspach, A. Bischof, J. A. C. Bland, G. Faini, U. Rüdiger, C. A. F. Vaz, L. Vila, and C. Vouille, Phys. Rev. Lett. **95**, 026601 (2005).
  - [14] G. S. D. Beach, C. Knutson, C. Nistor, M. Tsoi, and J. L. Erskine, Phys. Rev. Lett. **97**, 057203 (2006).
  - [15] M. Hayashi, L. Thomas, Ya. B. Bazaliy, C. Rettner, R. Moriya, X. Jiang, and S. S. P. Parkin, Phys. Rev. Lett. **96**, 197207 (2006).
  - [16] L. Berger, Phys. Rev. B **33** 1572 (1986). For a recent work, see S. E. Barnes, J. Ieda and S. Maekawa, Appl. Phys. Lett. **89**, 122507 (2006).
  - [17] M. V. Berry, Proc. R. Soc. London, Ser. A **392**, 45 (1984).
  - [18] G. Sundaram and Q. Niu, Phys. Rev. B **59**, 14915 (1999).
  - [19] A. P. Malozemo and J. C. Slonczewski, *Magnetic Domain Walls in Bubble Materials* (Academic Press, New York, 1979).
  - [20] Private communication with S. Zhang.
  - [21] R. D. McMichael and M. J. Donahue, IEEE Trans. Magn. **33**, 4167 (1997).
  - [22] J. Shibata, Y. Nakatani, G. Tatara, H. Kohno, Y. Otani, Phys. Rev. B **73**, 020403(R) (2006).
  - [23] J. He, Z. Li and S. Zhang, Phys. Rev. B **73**, 184408 (2006).
  - [24] Y. Nakatani, A. Thiaville and J. Miltat, Nature Mater. **2**, 521 (2003).
  - [25] O. Tchernyshyov and G.-W. Chern, Phys. Rev. Lett. **95**, 197204 (2005).
  - [26] G. S. D. Beach, C. Nistor, C. Knutson, M. Tsoi, and J. L. Erskine, Nat. Mater. **4**, 741 (2005).